

ONE-DIMENSIONAL NUMERICAL MODEL FOR PREDICTION OF JETSAM CONCENTRATION IN SEGREGATING FLUIDIZED BEDS

by

Mohamed Sobhi AL-AGHA^{a,b} and Pal SZENTANNAI^{a*}

^a Department of Energy Engineering, Faculty of Mechanical Engineering,
Budapest University of Technology and Economics (BME), Budapest, Hungary

^b Department of Mechanical Engineering, Faculty of Engineering,
Kafrelsheikh University, Kafrelsheikh, Egypt

Original scientific paper

<https://doi.org/10.2298/TSCI170418066A>

The present study introduces an advanced numerical solution of the so-called Gibilaro and Rowe equations to describe jetsam axial distribution in stationary fluidized beds. The proposed model takes into account the mechanisms responsible for jetsam movement in binary fluidized beds. This methodology benefits from the recent availability of high computational units in optimizing model coefficients to give the best fit with the experimental data. Fortunately, there is a large number of experimental test cases from literature, that can help with scaling the model. In such a way, the model has been calibrated via more than 50 experimental cases of different binary mixtures at various operating conditions. Therefore, it can be considered as a reliable predicting tool for various compositions and operating conditions of fluidized beds in many industrial applications. Also, comparisons with previously published models have been done. The results have shown that the proposed numerical model is in good agreement with the experimental data.

Key words: numerical solution, Gibilaro and Rowe model, binary mixture, fluidized beds, model calibration

Introduction

Binary mixtures in fluidized beds represent the real situation in most industrial and power generation applications. The existence of two or more granular materials of different densities and/or of different sizes has a completely different view compared to mono density and size materials in the fluidization process. The phenomena of mixing and segregation of binary mixtures were experimentally examined in several studies. Recently, on the one hand, with the availability of high speed computational facilities and it becomes easier to simulate very complex phenomena with reliable accuracy. The 1-D, 2-D, and 3-D models were developed to give more descriptive information about mixing and segregation of binary mixtures. This information can help in scaling from pilot scale test-rig to real fluidized beds.

On the other hand, it requires, in addition to higher computational facilities, a long time for 2-D and 3-D simulations of multicomponent particulate solids in fluidized beds. This problem predicts the need for the improvement of the 1-D solutions in parallel to give a reasonable accuracy compared to 2-D and 3-D systems, especially when the study is focusing on a certain phenomenon, such as segregation. One of the best models describing the segregation

* Corresponding author, e-mail: szentannai@energia.bme.hu

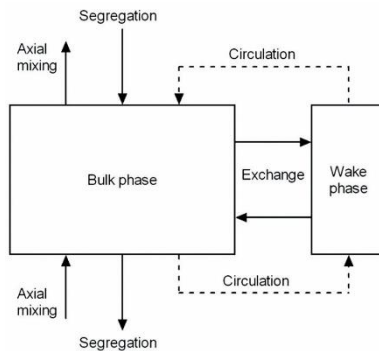


Figure 1. Schematic diagram of segregation mechanisms of the G-R model [1]

phenomenon was established by Gibilaro and Rowe [1]. This model was constructed on the basis of the two-phase theory, *i. e.* considering the existence of the particulate material in the bulk and wake phases to indicate the interaction between the bed material and the fluidization bubbles as shown in fig. 1. The model described the movement of the jetsam particle (the material which tends to segregate to the bed bottom during fluidization [2]) based on four essential mechanisms, see fig. 1.

Gibilaro and Rowe (G-R) [1] proposed three different analytical solutions for their model equations, namely Case 1, Case 2, and Case 3. In each of them they neglected the effect of one of the four mechanisms responsible for the mixing and the segregation phenomena. For example, they disregarded the influence of axial dispersion

in Case 2, compared to the exchange between the two phases. After this step, a lot of efforts were carried out to assign G-R model parameters to the physical variables corresponding to real operations, such as mixture composition, bed geometry, and fluidization velocity. Chiba and Kobayashi [3], Chiba *et al.* [4] and Tanimoto *et al.* [5] elaborated mathematical approaches for estimating G-R model parameters. Their calculations were based on the segregation distance of jetsam created by single bubble passage as a function of particle size and density ratios of the mixture. In addition, these calculations also considered the fluidization bubble characteristics from correlations that were described earlier by Nicklin [6] and Kato and Wen [7].

Naimer *et al.* [8] used these correlations to link the physical operation variables to the G-R model parameters in order to apply a general solution to a wide range of operating conditions. However, they could not find an estimation for an axial dispersion coefficient. Thus, they used the G-R solution which neglected the effect of axial mixing (Case 2) to simulate jetsam concentration in the fluidized bed. Nevertheless, their model showed limitations with higher total jetsam weight fractions ($x_j \geq 0.5$) due to axial dispersion of solids being ignored. It was reported by Garcia *et al.* [9] that the effect of axial mixing cannot be neglected. They used the Gibilaro and Rowe [1] analytical solutions (Case 1 and Case 3) that regarded axial dispersion mechanism, in their comparison, with experimental data. It was proven that the model can give a good agreement if a modified set of coefficient values is introduced in the process. But, it was not understood how to choose the suitable analytical solution (Case 1 or Case 2) in the absence of experimental data. The efforts of Hoffman and Romp [10], and Hoffman *et al.* [11] showed that the model was able to give good predictions without requiring adjustable parameters if suitable correlations had been applied. Abanades *et al.* [12], and Hartholt [13] used numerical solutions of the G-R model based on the initial boundary value problem, and the boundary value problem for slugging and bubbling bed, respectively. The last trial for the full numerical solution of the G-R model was done by Leaper *et al.* [14]. The test was accounting for all mechanisms responsible for mixing and segregation in the bubbling fluidized beds. But they applied their solution only on one set of experimental results, on their own measurements.

In general, the problem of using equations and correlations from literature to estimate the G-R model coefficient is that all the previous correlations have moderate accuracy in addition to the limited ranges based on the original experimental investigations. However, the

G-R is a 1-D model, therefore, it is very sensitive to the value of model coefficients. Thus, the objective of the present study is to improve the G-R full numerical solution model using experimental data by calibration. For this reason, a large set of experimental cases from the literature of different mixture compositions at a wide range of fluidization velocities (58 cases) has been utilized for model scaling.

Optimizing the G-R model

The G-R model

The G-R model [1] was constructed based on the two-phase theory of Toomey and Johnstone [15], which was originally derived by describing the solids movement in the fluidization process by the action of the rising bubbles. The bubbles circulate the solids by separating it into two phases. One portion of the solids is drawn to the upper layers of the bed with the bubbles (wake phase), and the rest is reacting to refill the volume which was occupied by the rising bubbles (bulk phase). The theory was applied to binary fluidized beds containing heavier particles of high density and/or size (jetsam) and lighter particles of small density and/or size (flotsam). The G-R model is based on the following assumptions:

- the space occupied by the bubbles is ignored,
- the volumetric flow rate of solids is constant along all horizontal planes through the bed,
- the amount of segregation occurring at any point is proportional to the jetsam concentration at that particular point, and
- the jetsam transport in the binary bed is caused by four mechanisms (see fig. 1): axial *mixing*, axial *segregation*, *circulation* at the top and bottom of the bed, and *exchange* between the bulk and wake phases.

Based on the previous assumptions, jetsam balances can be formulated on a typical bed element of height dZ for both phases considering all four jetsam transport mechanisms. The differential equations derived from these two elemental balances become [1]:

$$\beta \frac{\partial^2 C_B}{\partial Z^2} + (\lambda + 1 - 2C_B) \frac{\partial C_B}{\partial Z} + \gamma \lambda (C_w - C_B) = 0 \quad (1)$$

$$\lambda \frac{\partial C_w}{\partial Z} + \gamma \lambda (C_B - C_w) = 0 \quad (2)$$

where C_B and C_w are the jetsam concentration in the bulk and wake phases along the axial direction, respectively, and β , γ , and λ are further analytical parameters. They are defined in the paper setting up this theoretical model [1], and their phenomenological essences can be summarized:

- the β provides a measure of the rate of *axial mixing* relative to the rate of *segregation* as a fraction of volumetric flow rates,
- the γ is the ratio of the bulk/wake *phase exchange* volume flow rate and solid *circulation* volume flow rate, and
- the λ is the fraction of solid *circulation* volume flow rate and *segregation* volume flow rate.

Consequently, the average volume and mass concentrations of jetsam can be calculated [1]:

$$C_{ave} = (1 - f_w)C_B + f_w C_w \quad (3)$$

$$X_{\text{ave}} = \frac{C_{\text{ave}} \frac{\rho_j}{\rho_f}}{1 - \left(1 - \frac{\rho_j}{\rho_f}\right) C_{\text{ave}}} \quad (4)$$

where f_w is the volumetric fraction of all solids in the wake phase.

Gibilaro and Rowe [1] made some mathematical simplifications for solving these differential equations analytically by ignoring one or two mechanisms in each case. In this way, they extracted three analytical solutions, namely Case 1, Case 2, and Case 3. In each of them they neglected one or two of the mechanisms responsible for the mixing/segregation phenomena. A brief overview and re-representation of these cases is given in *Appendix A*.

The present numerical solution

We propose and introduce an overall numerical solution of eqs. (1) and (2) on the basis of the 4th order Runge-Kutta method (initial boundary value problem, see Nakamura [16]). The initial boundary values for the bulk and wake jetsam concentrations, as well as the bulk phase gradient at the bottom of the bed ($Z = 0$), are estimated from eqs. (A5), (A6), and (A7) as in the G-R analytical solution (Case 3, *Appendix A*):

$$\frac{\partial C_B}{\partial Z} \Big|_{Z=0} = \frac{C_{B0}(1 - C_{B0})}{\beta} \quad (5)$$

$$C_{w0} = C_{B0} \quad (6)$$

where C_{w0} and C_{B0} are the wake and bulk phases concentration at the bottom of the bed.

Model calibration

The model calibration procedure is shown in fig. 2, clarifying the sequence of the individual calculation steps. As visible, this is a loop of iteration in four variables, and it internally includes the numerical solving of the set of differential eqs. (1) and (2). The variables of the external loop are the analytical parameters β , γ , and λ of the differential equations, and f_w , the parameter of the algebraic eq. (3).

It is to mention here that the goal of the current work is to calculate the best fitting values of these four free parameters of the G-R model. These parameters are strongly influenced by many physical parameters of the particular experimental set-up (fluidization velocity, fluidization number, *e. g.*), however, formulating these dependencies is beyond the scope of the actual paper.

This method uses the actual standard deviation value, which is defined:

$$\sigma_{\text{st}} = \sqrt{\frac{\sum_{i=1}^n (C_{\text{ave},i} - C_{\text{ave},m})^2}{n-1}} \quad (7)$$

where $C_{\text{ave},i}$ and $C_{\text{ave},m}$ are the numerical and experimental average jetsam concentration values at a given point, respectively, while n is the number of data points, the standard deviation would be calculated for. The vital role of using experimental data in identifying the optimum model coefficients is evident, and it is also clearly visible in this figure.

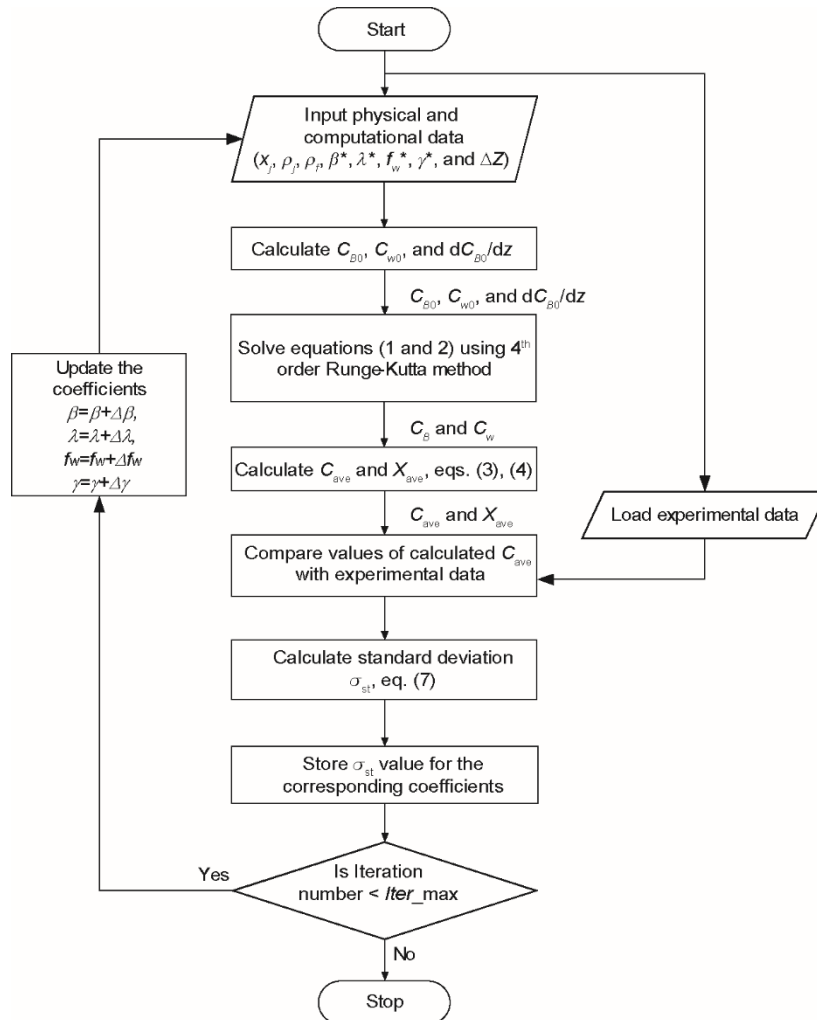


Figure 2. Flow chart of the calibration procedure of the proposed model

The data were taken from a high number of available publications so that the best fit with true experiments could be reached, and the entire procedure could be verified. While a similar procedure of varying the analytical model parameters was carried out by Garcia *et al.* [9], and although the fit found was very much appropriate in some cases, in several other cases only low accuracy could be reached.

An additional general problem of these approaches is that the experimental data are sometimes not fully available, consequently it cannot be decided whether the actual case is subject to the theoretical models of Case 1 or Case 3. This leads to the necessity of formulating a general and applicable full numerical solution that can be valid over a considerable range of operating conditions. The results of this general numerical model can be seen in the next section.

Results and outlook

The results of the calibration and validation procedure of the previous model on all the published data found are summarized in tab. 1. This table shows the set of model coefficients that fit best with the experimental data from literature for different mixture compositions and fluidization velocities. The optimized-coefficient solutions, see figs. 3-5, fit very

Table 1. The G-R model coefficients of best fit with experimental data from literature

#	Experimental conditions								Best fit model parameters				Ref.
	x_j [-]	ρ_i [kgm ⁻³]	ρ_f [kgm ⁻³]	d_j [mm]	d_f [mm]	H [m]	D [m]	u [ms ⁻¹]	β [-]	λ [-]	f_w [-]	γ [-]	
1	0.10	8860	2950	0.273	0.461	–	0.147	0.336	0.012	0.001	0.001	0.050	[8]
2	0.20	2476	1064	0.231	0.231	–	0.120	0.059	0.0085	0.040	0.050	0.950	[18]
3	0.25	2476	1064	0.116	0.275	–	0.184	0.036	0.012	0.060	0.035	0.850	
4	0.25	2200	1400	4.000	4.000	–	0.114	1.600	0.002	0.210	0.033	0.300	[9]
5	0.25	1400	920	4.000	4.000	–	0.114	1.380	0.004	0.250	0.200	0.050	
6	0.25	2200	920	4.000	4.000	–	0.114	1.420	0.003	0.680	0.006	0.020	
7	0.25	2476	2476	0.116	0.275	–	0.184	0.062	0.007	0.150	0.110	0.050	[18]
8	0.25	2476	1064	0.11	0.275	–	0.184	0.066	0.012	0.075	0.001	0.200	
9	0.40	8860	2950	0.273	0.461	–	0.147	0.337	0.020	0.052	0.005	0.750	[8]
10	0.40	8860	2950	0.273	0.461	–	0.147	0.650	0.015	0.075	0.125	0.850	
11	0.50	8750	2510	0.235	0.565	0.160	0.146	0.290	0.016	0.130	0.005	0.500	[11]
12	0.50	8750	2510	0.235	0.565	0.160	0.146	0.330	0.014	0.140	0.045	0.500	
13	0.50	2200	1400	4.000	4.000	–	0.114	1.600	0.034	0.135	0.001	0.950	[9]
14	0.50	1400	920	4.000	4.000	–	0.114	1.300	0.012	0.100	0.010	0.800	
15	0.50	2200	920	4.000	4.000	–	0.114	1.460	0.036	0.110	0.020	0.950	
16	0.50	2200	920	4.000	4.000	–	0.114	1.180	0.058	0.120	0.002	0.300	
17	0.50	2200	920	4.000	4.000	–	0.114	1.300	0.024	0.350	0.270	0.950	
18	0.50	2200	920	4.000	4.000	–	0.114	1.370	0.036	0.110	0.020	0.950	
19	0.50	2200	920	4.000	4.000	–	0.114	1.460	0.003	0.120	0.310	0.100	
20	0.50	2200	1400	4.000	4.000	–	0.114	1.680	0.015	0.200	0.270	0.950	
21	0.50	8650	2490	0.273	0.281	0.082	0.146	0.282	0.015	0.350	0.090	0.850	
22	0.50	8650	2490	0.273	0.281	0.082	0.146	0.298	0.015	0.200	0.270	0.950	
23	0.50	8650	2490	0.273	0.281	0.082	0.146	0.312	0.015	0.200	0.280	0.950	
24	0.50	8650	2490	0.273	0.281	0.082	0.146	0.327	0.020	0.400	0.100	0.500	[13]
25	0.50	8650	2490	0.273	0.281	0.082	0.146	0.346	0.016	0.280	0.270	0.550	
26	0.50	11320	2490	0.112	0.281	0.120	0.146	0.119	0.038	0.290	0.140	0.950	



Table 1. Continuations

#	Experimental conditions								Best fit model parameters				Ref.
	x_j [-]	ρ_i [kgm ⁻³]	ρ_f [kgm ⁻³]	d_j [mm]	d_f [mm]	H [m]	D [m]	u [ms ⁻¹]	β [-]	λ [-]	f_w [-]	γ [-]	
27	0.50	11320	2490	0.112	0.281	0.120	0.146	0.146	0.012	0.195	0.005	0.400	
28	0.50	11320	2490	0.112	0.281	0.120	0.146	0.174	0.040	0.030	0.470	0.950	[13]
29	0.50	11320	2490	0.112	0.281	0.120	0.146	0.190	0.020	0.370	0.300	0.250	
30	0.50	11320	2490	0.112	0.281	0.120	0.146	0.255	0.015	0.200	0.280	0.950	
31	0.50	2476	1064	0.116	0.275	–	0.120	0.045	0.016	0.270	0.018	0.850	
32	0.50	2476	2476	0.231	0.116	–	0.120	0.054	0.012	0.050	0.470	0.050	
33	0.50	2476	2476	0.231	0.116	–	0.180	0.054	0.0095	0.390	0.180	0.050	
34	0.50	2476	1064	0.231	0.231	–	0.120	0.076	0.022	0.120	0.060	0.500	
35	0.50	2476	1064	0.116	0.275	–	0.184	0.049	0.019	0.250	0.015	0.600	[18]
36	0.69	2476	1064	0.116	0.275	–	0.184	0.029	0.020	0.490	0.015	0.950	
37	0.69	2476	1064	0.116	0.275	–	0.184	0.038	0.016	0.450	0.005	0.350	
38	0.69	2476	1064	0.116	0.275	–	0.184	0.045	0.010	0.380	0.140	0.200	
39	0.69	2476	1064	0.116	0.275	–	0.184	0.056	0.016	0.130	0.410	0.850	
40	0.50	4500	2600	0.180	0.120	–	0.150	0.017	0.012	0.620	0.070	0.300	
41	0.50	4500	2600	0.180	0.120	–	0.150	0.022	0.012	0.060	0.035	0.850	[14]
42	0.50	4500	2600	0.180	0.120	–	0.150	0.034	0.019	0.250	0.015	0.600	
43	0.50	4500	2600	0.180	0.120	–	0.150	0.030	0.020	0.500	0.120	0.850	
44	0.70	8860	2950	0.273	0.461	–	0.147	0.336	0.055	0.008	0.075	0.950	[8]
45	0.75	8750	2510	0.235	0.565	0.160	0.146	0.525	0.010	0.090	0.410	0.900	[11]
46	0.75	2200	1400	4.000	4.000	–	0.114	1.610	0.116	0.230	0.200	0.900	
47	0.75	2200	1400	4.000	4.000	–	0.114	1.690	0.046	0.370	0.100	0.200	
48	0.75	1400	920	4.000	4.000	–	0.114	1.120	0.062	0.010	0.490	0.050	
49	0.75	1400	920	4.000	4.000	–	0.114	1.300	0.062	0.130	0.500	0.050	
50	0.75	1400	920	4.000	4.000	–	0.114	1.500	0.008	0.250	0.340	0.100	[9]
51	0.75	2200	920	4.000	4.000	–	0.114	1.380	0.020	0.052	0.005	0.750	
52	0.75	2200	920	4.000	4.000	–	0.114	1.380	0.015	0.075	0.125	0.850	
53	0.75	2200	920	4.000	4.000	–	0.114	1.600	0.012	0.001	0.001	0.050	
54	0.75	2200	920	4.000	4.000	–	0.114	1.700	0.055	0.005	0.075	0.950	
55	0.75	2476	2476	0.231	0.116	–	0.120	0.042	0.012	0.180	0.700	0.050	
56	0.75	2476	1064	0.231	0.231	–	0.120	0.078	0.0115	0.620	0.070	0.300	[18]
57	0.75	2476	1064	0.116	0.275	–	0.184	0.028	0.018	0.560	0.040	0.800	
58	0.75	2476	1064	0.116	0.275	–	0.184	0.051	0.003	0.410	0.290	0.100	

well with the experimental data of different operating conditions. It was not possible, however, to show graphically all the model-fitting results. That is why a systematic selection was

concluded with the goal of showing representative diagrams on a wide range of cases and experimental parameter values.

Figure 3 shows markedly mixed cases of different fluidized bed systems under significantly diverse operating conditions. A characteristic of this situation is the almost vertical concentration profile along the bed height.

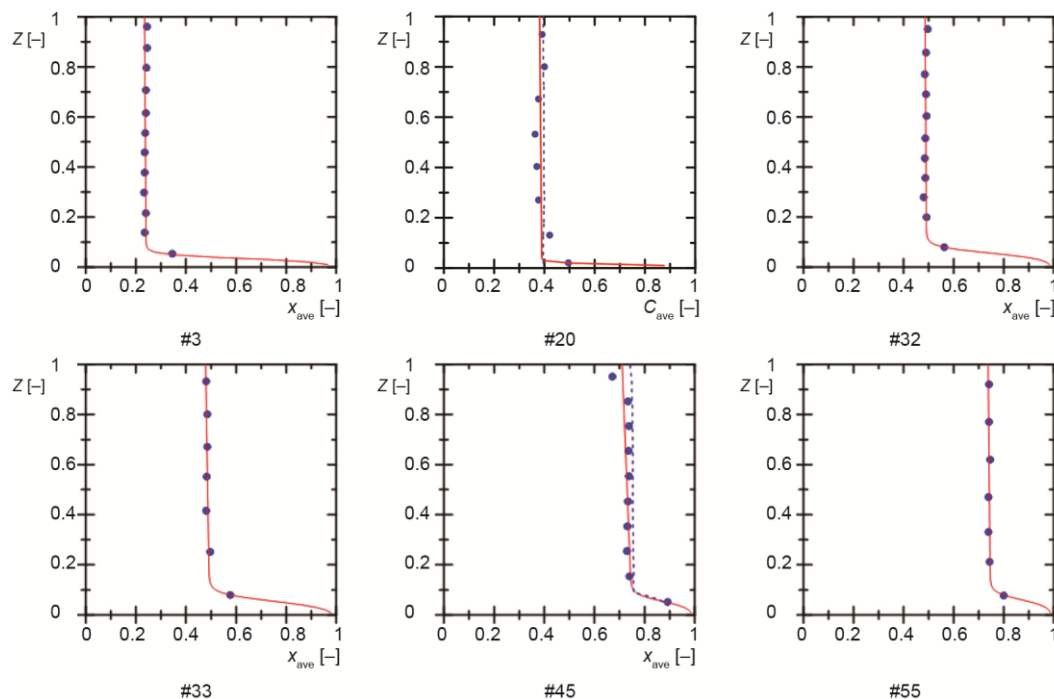


Figure 3. Sample results of the present model (continuous lines) together with the experimental data points (symbols) in some markedly mixed cases. If the original paper also includes an own model it is shown by dashed lines. Experimental conditions given in tab. 1, the first column of which (#) are referenced by the previous subfigure identifiers

Figure 4, on the other hand, shows markedly segregated cases. A common characteristic of these concentration profiles are their sharp s-shaped appearances indicating a separation line between the jetsam-rich zone at the bottom and the flotsam-rich zone on the top. The vertical position of the central point of this separation line is called the segregation distance or the height of the jetsam-rich layer.

The model of the present study is also capable for describing the intermediate cases between the markedly mixed and markedly segregated ones, as shown in fig. 5. The concentration profiles are rather complex in these cases, containing inclined (not vertical) lines and denser bottom jetsam concentrations.

An useful overview of the results would be a systematic change of single parameters at a time, of course. It could be done on the model itself, but we always wanted to compare the calculated results with measured data. Because the big number of published experiments we are referring to were not carried out according to this logic, such a pure visualization of the effects cannot be done here. However, some effects of the most important experimental parameter changes can be well observed on the concentration profiles shown in figs. 3-5 as

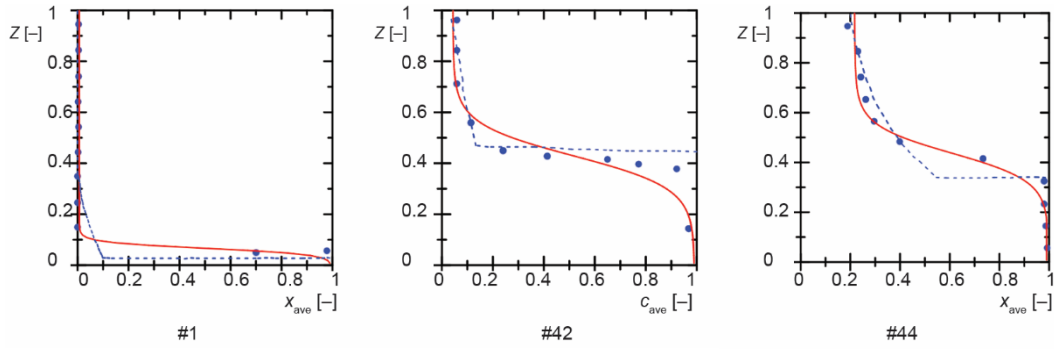


Figure 4. Sample results of the present model (continuous lines) together with the experimental data points (symbols) in some markedly segregated cases. If the original paper also includes an own model it is shown by dashed lines. Experimental conditions given in tab. 1, the first column of which (#) are referenced by the previous subfigure identifiers

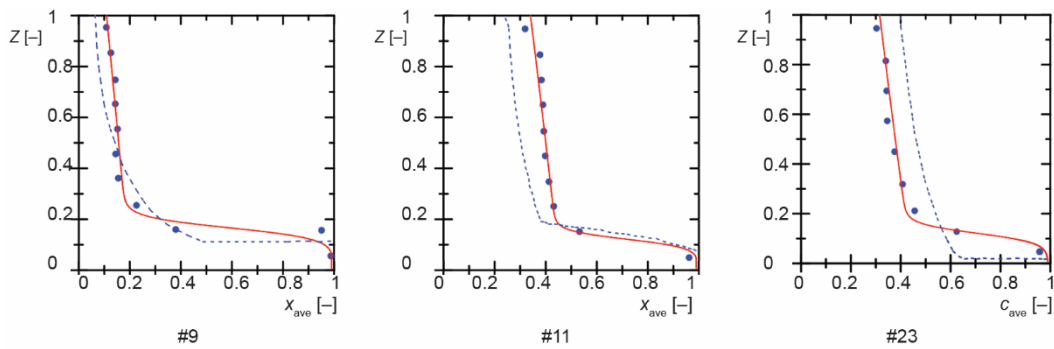
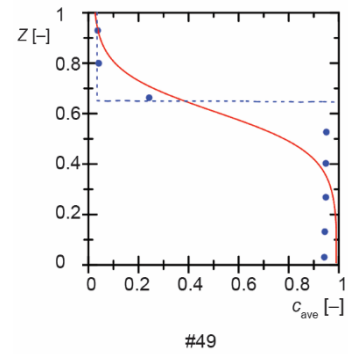
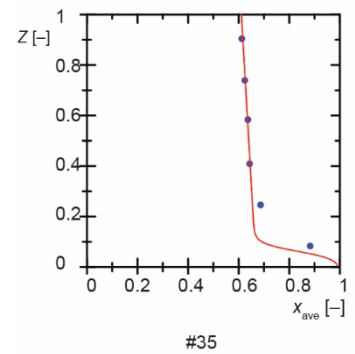


Figure 5. Sample results of the present model (continuous lines) together with the experimental data points (symbols) in some intermediate mixing/segregation cases. If the original paper also includes an own model it is shown by dashed lines. Experimental conditions given in tab. 1, the first column of which (#) are referenced by the previous subfigure identifiers



follows. (For better visualization they could be put next to each other, however, we did not want to increase the length of this paper by such repeated representations of existing diagrams.) The effect of fluidization velocity can be observed by comparing subfigures #20 and #49 (of figs 3-5) *e. g.*, which clearly show that an increased velocity results in an advanced mixing. The effect of particle size ratio d_j/d_f was studied before experimentally [17] and found to be an almost negligible influence compared to the particle density ratio ρ_j/ρ_f , as clearly recognizable by comparing subfigures #32 and #20. A similarly negligible effect is the bed diameter, as visible by comparing the cases #32 and #33.

The versatility of the cases found and used for validating the present model can be further illustrated by mentioning that cases #20, #45, and #49 are characterized by high fluidization velocities, while case #3, #42, and #57 demonstrate the opposite end. The overall jet-sam concentration in the selected cases range from 0.1 in #1 through 0.5 in #11 up to 0.75 in #45.

Throughout the numerical calibration process, it was observed that the present application of the G-R model is very sensitive to both model coefficients and initial values of the variables under numerical integration. Thus, better predictions can be achieved if more proper initial boundary conditions can be introduced, that is, better estimates for the initial bulk and wake volume fractions C_{B0} , C_{w0} , and the initial bulk axial gradient $dC_B/dz|_0$.

As an outlook towards further development of the G-R model, its generalization can be mentioned. The main goal of the development is to find a general and applicable integration method realizing a link between the model parameters and the physical operational parameters. Fortunately, previous studies have clarified the influence of most of these parameters, such as fluidization velocity, mixture composition, and bed geometry. The problem faced is that, in many cases, some important parameters, such as bed aspect ratio, bed cross-section, and minimum fluidization velocities have not clearly been given in the investigated publications. Moreover, calculating their estimated values on the basis of available geometrical data, densities, and other characteristics, is a rather difficult task. For example, we have tested three commonly used correlations on the basis of a paper [16] to determine the minimum fluidization velocity of two granular materials with both the measured u_{mf} values and the data required by the predicting equations. Table 2 in *Appendix B* shows the predictions of each equation and the relative errors compared to their measured data. It is clear from this table that the absolute error of these correlations (ranging from -98% to +95%) makes them unreliable in the investigated cases, due to this absolutely vital parameter, the minimum fluidization velocity. Thus, the best way to overcome this problem seems to have our own measurements on the same bed material.

Conclusions

In the present study, a full numerical solution of the G-R model was introduced and demonstrated. The model was calibrated by using a large set of experimental data from previously published works applicable for different bed compositions and fluidization velocities. The study also included comparisons with other theoretical models from literature, and the present model proved a significant step forward in the field.

The key improvements and benefits of the presented model compared to the available ones including the G-R model are the following.

- It considers all four mechanisms described in the theoretical G-R model. (The analytical solutions always neglect some of them to make the integration possible.)
- It contains an optimal parameter seeking procedure.

- It is applicable for all mixing/segregation cases covered by wide parameter ranges.
- It performs better in many cases – especially in the intermediate mixing/segregation cases.

It was also observed that the G-R model accuracy is very sensitive to the model coefficients and the initial boundary conditions.

To make a more general and applicable solution in the future, a mathematical link between the model coefficient and the physical parameter should be established. The present study was an important step towards this purpose, and it became evident that the main obstacle, in most cases, was lying in the shortage of the descriptive conditions of the previously published works. For example, very few studies reported on the minimum fluidization velocity, even though this is a much important variable related to the model coefficient. Although there is a large number of existing studies on correlating equations for minimum fluidization velocity available, in general, in most cases they cannot be applied due to their high deviation.

Nomenclature

C – local jetsam volume fraction, [–]	μ – dynamic viscosity, [Pa.s]
D – bed diameter, [m]	β – coefficient of jetsam concentration axial gradient ($= r/kH$), [–]
d – particle diameter, [mm]	γ – phase exchange to circulation coefficient ($= qH/w$), [–]
f_j – total volumetric fraction of jetsam in the bed, [–]	ε – bed porosity, [–]
f_w – volumetric fraction of solids in the wake phase, [–]	λ – circulation to segregation coefficient ($= w/k$), [–]
g – coefficient of jetsam concentration term ($C_B - C_w$), [–]	ρ – bulk density, [kgm ⁻³]
H – total bed height, [m]	σ – standard deviation, [–]
k – segregation coefficient, [m ³ s ⁻¹]	<i>Subscripts</i>
q – exchange coefficient, [m ³ s ⁻¹]	ave – average
r – axial mixing coefficient, [m ³ s ⁻¹]	B – in the bulk phase
U – velocity, [ms ⁻¹]	f – flotsam
u – fluidization velocity, [ms ⁻¹]	g – gas
u_{mf} – minimum fluidization velocity, [ms ⁻¹]	j – jetsam
w – circulation coefficient, [m ³ s ⁻¹]	mf – minimum fluidization
X – local jetsam mass fraction, [–]	p – particle
x_j – total jetsam weight fraction in the mixture, [–]	w – in the wake phase
Z – dimensionless bed height, [–]	
<i>Greek symbols</i>	
φ_s – particle's sphericity, [–]	

Appendix A. Analytical solution cases of the G-R model

To allow analytical solving of the G-R model eqs. (1) and (2) [1], in some practical cases, they proposed a portion of mathematical simplifications by ignoring one or two mechanisms. A brief overview and re-representation of these cases is given in this *Appendix*.

Case 1, Negligible axial mixing and phase exchange

Case 1A, Vigorous fluidization

In a vigorously fluidized system the influence of both axial mixing and phase exchange can be supposed to be negligible compared to circulation and segregation. In this case the jetsam concentration is [1]:

$$C_B = \frac{1}{2} \left\{ 1 + \frac{\lambda}{f_w} + \sqrt{\left(1 + \frac{\lambda}{f_w}\right)^2 - \frac{4f_j\lambda}{f_w}} \right\} \quad (\text{A1})$$

$$C_w = C_B + \frac{C_B}{\lambda} (1 - C_B) \quad (\text{A2})$$

$$f_j = \frac{1}{1 + \left(\frac{1}{x_j} - 1\right)^{\frac{\rho_j}{\rho_f}}} \quad (\text{A3})$$

where f_j and x_j are the total volumetric fraction, total weight fraction of jetsam present in the bed, while ρ_j and ρ_f are the bulk densities of jetsam and flotsam, respectively.

Case 1B, Weak fluidization

In this case there is only one parameter controlling the concentration regimes namely critical bed height, Z^* , which is defined by:

$$Z^* = \frac{(f_j - f_w) - \lambda(1 - f_w)}{(1 - f_w)(1 - \lambda)} \quad (\text{A4})$$

Thereafter, the jetsam concentration can be calculated [1]:

$$Z^* > Z \geq 0, \quad C_B = 1$$

$$Z = Z^*, \quad C_B = (\lambda + 1)/2$$

$$1 \geq Z > Z^*, \quad C_B = \lambda$$

Case 2, The additional effect of exchange between the phases

In this case, eq. (1) is integrated, neglecting the effect of the axial mixing compared to the exchange between the two phases. Therefore, the jetsam distribution will be [1]:

$$\left(\frac{C_B}{\lambda}\right)^{1+\lambda} \left(\frac{1-C_B}{1-\lambda}\right)^{1-\lambda} = e^{-\gamma(Z-Z^*)} \quad (\text{A5})$$

where λ is the circulation/segregation coefficient.

Case 3, The effect of axial mixing in the bulk phase

By neglecting the exchange term $\gamma\lambda(C_w - C_B)$, eq. (1) reduced to the following simplified differential equation [1]:

$$\beta \frac{\partial^2 C_B}{\partial Z^2} + (\lambda + 1 - 2C_B) \frac{\partial C_B}{\partial Z} = 0 \quad (\text{A6})$$

where

Table 2. Accuracy of minimum fluidization velocity predictions using correlations from literature

Reference measurements					
	Measurement details	u_{mf} measured, [ms ⁻¹]		u_{mf} measured, [ms ⁻¹]	
	$\rho_s = 2476 \text{ kg/m}^3$; $\rho_g = 1 \text{ kg/m}^3$; $d_p = 0.116 \text{ mm}$; $\mu_g = 1.83\text{e-}5 \text{ Pa}\cdot\text{s}$; lead-free glass Further details, reference: [16]	0.018			
	$\rho_s = 1064 \text{ kg/m}^3$; $\rho_g = 1 \text{ kg/m}^3$ $d_p = 0.231 \text{ mm}$; $\mu_g = 1.83\text{e-}5 \text{ Pa}\cdot\text{s}$ Polystyrene Further details, reference: [16]			0.029	
Predicting equations and relative errors					
Ref	Equation	u_{mf} predicted, [ms ⁻¹]	error	u_{mf} predicted, [ms ⁻¹]	error
[19]	$u_{mf} = \frac{\mu_g}{\rho_g d_p} \left\{ \left[33.7^2 + 0.0408 \frac{d_p^3 \rho_g (\rho_s - \rho_g)}{\mu_g^2} \right]^{\frac{1}{2}} - 33.7 \right\}$	0.0011	-93.9%	0.0019	-93.5%
[20]	$u_{mf} = \frac{\mu_g}{\rho_g d_p} \left\{ \frac{-150(1 - \varepsilon_{mf})}{3.5\varphi_s} \left(\frac{-150(1 - \varepsilon_{mf})}{3.5\varphi_s} \right)^2 + \frac{\varphi_s \varepsilon_{mf}^3 g d_p^3 \rho_g (\rho_s - \rho_g)}{1.75 \mu_g^2} \right\}$	0.0334	+85.5%	0.0565	+94.9%
[21]	– for glass: $u_{mf} = (4.3384 \cdot 10^{-7}) \left[\frac{g d_p^2 (\rho_s - \rho_g)}{\mu_g} \left(\frac{\rho_s}{\rho_g} \right)^{1.23} \right]^{0.89029 \pm 0.18880}$ – for polystyrene: $u_{mf} = (2.1308 \cdot 10^{-4}) \left[\frac{g d_p^2 (\rho_s - \rho_g)}{\mu_g} \left(\frac{\rho_s}{\rho_g} \right)^{1.23} \right]^{0.59460 \pm 0.01730}$	0.0005	-97.3%	0.0172	-40.8%

$$C_B = \frac{1}{2} \left[\lambda + 1 + P \left(\frac{1 + B_2 e^{\frac{ZP}{\beta}}}{1 - B_2 e^{\frac{ZP}{\beta}}} \right) \right] \quad (A7)$$

$$P = [(\lambda + 1)^2 - 4\lambda C_{B0}]^{\frac{1}{2}} \quad (\text{A8})$$

$$B_2 = \frac{\lambda + 1 - 2C_{B0} + P}{\lambda + 1 - 2C_{B0} - P} \quad (\text{A9})$$

$$C_{B0} = \frac{1}{f_w} \left[f_j - (1 - f_w) \left(\frac{\lambda + 1 + P}{2} - \beta \ln \frac{1 - B_2 e^{\frac{P}{\beta}}}{1 - B_2} \right) \right] \quad (\text{A10})$$

Appendix B. Review of models for predicting u_{mf} , minimum fluidization velocity

Due to the lack of the minimum fluidization velocity data on mixing and segregation in binary fluidized beds in most publications, a calculation method to determine them is necessary. Table 2 gives an overview of the models found in the literature. This table also comprises a comparison of predictions with some available measured data of each model, taken also from the literature. It seems to be evident from this table that the absolute error of these correlations (ranging from -98% to +95%) makes it very difficult to substitute the lacking u_{mf} data by predicted ones in order to develop a mixing-segregation model.

References

- [1] Gibilaro, L. G., Rowe, P. N., A Model for a Segregating Gas Fluidised Bed, *Chemical Engineering Science*, 29 (1974), 6, pp. 1403-1412
- [2] Rowe, P. N., Nienow, A. W., Particle Mixing and Segregation in Gas Fluidised Beds. A Review, *Powder Technology*, 15 (1976), 2, pp. 141-147
- [3] Chiba, T., Kobayashi, H., Solid Exchange between the Bubble Wake and the Emulsion Phase in a Gas-fluidised Bed, *Journal of Chemical Engineering of Japan*, 10 (1977), 3, pp. 206-210
- [4] Chiba, S., et al., Measurement of Solid Exchange between the Bubble Wake and the Emulsion Phase in a Three-Dimensional Gas-Fluidised Bed, *Journal of Chemical Engineering of Japan*, 12 (1979), 1, pp. 43-45
- [5] Tanimoto, H., et al., Jetsam Descent Induced by a Single Bubble Passage in Three-Dimensional Gas-fluidized Beds, *Journal of Chemical Engineering of Japan*, 14 (1981), 4, pp. 273-276
- [6] Nicklin, D. J., Two-Phase Bubble Flow, *Chemical Engineering Science*, 17 (1962), 9, pp. 693-702
- [7] Kato, K., Wen, C.Y., Bubble assemblage model for fluidized bed catalytic reactors, *Chemical Engineering Science*, 24 (1969), 8, pp. 1351-1369
- [8] Naimer, N. S., et al., Parameter Estimation for a Solids Mixing|Segregation Model for gas Fluidised Beds, *Chemical Engineering Science*, 37 (1982), 7, pp. 1047-1057
- [9] Garcia-Ochoa, F., et al., A Study of Segregation in a Gas-Solid Fluidized Bed: Particles of Different Density, *Powder Technology*, 58 (1989), 3, pp. 169-174
- [10] Hoffmann, A. C., Romp, E. J., Segregation in a Fluidised Powder of a Continuous Size Distribution, *Powder Technology*, 66 (1991), 2, pp. 119-126
- [11] Hoffmann, A. C., et al., Particle Segregation in Fluidised Binary Mixtures, *Chemical Engineering Science*, 48 (1993), 9, pp. 1583-1592
- [12] Abanades, J. C., et al., A Mathematical Model for Segregation of Limestone-Coal Mixtures in Slugging Fluidised Beds, *Chemical Engineering Science*, 49 (1994), 23, pp. 3943-3953
- [13] Hartholt, G. P., Particle Mixing in Gas Solid Fluidised Beds, Ph. D. thesis, Faculty of Science and Engineering, University of Groningen, Groningen, The Netherland, 1996
- [14] Leaper, M. C., et al., Total Solution of the Gibilaro and Rowe Model for a Segregating Fluidized Bed, *Chemical Engineering. Technology*, 30 (2007), 2, pp. 161-167
- [15] Toomey, R. O., Johnstone, H. F., Gaseous Fluidization of Solid Particles, *Chemical Engineering Prog.* 48 (1952), pp. 220-226

- [16] Nakamura, S., *Applied Numerical Methods with Software*, Prentice Hall, Englewood Cliffs, N. J, USA, 1991
- [17] Formisani, B., *et al.*, A Fundamental Approach to the Phenomenology of Fluidization of Size Segregating Binary Mixtures of Solids, *Chemical Engineering Science*, 56 (2001), 1, pp. 109-119
- [18] Joseph, G. G., *et al.*, Experimental Segregation Profiles in Bubbling Gas-Fluidized Beds, *AIChE Journal*, 53 (2007), 11, pp. 2804-2813
- [19] Wen, C. Y., Yu, Y. H., A Generalized Method for Predicting the Minimum Fluidization Velocity, *AIChE Journal*, 12 (1966), 3, pp. 610-612
- [20] Lippens, B. C., Mulder, J., Prediction of the Minimum Fluidization Velocity, *Powder Technology*, 75 (1993), 1, pp. 67-78
- [21] Coltters, R., Rivas, A. L., Minimum Fluidation Velocity Correlations in Particulate Systems, *Powder Technology*, 147 (2004), 1-3, pp. 34-48